Desalination 415 (2017) 8–13

Contents lists available at ScienceDirect

Desalination

journal homepage: www.elsevier.com/locate/desal

A one-dimensional model for water desalination by flow-through electrode capacitive deionization

Eric N. Guyes [a], Amit N. Shocron [a], Anastasia Simanovski [a], P.M. Biesheuvel [b], Matthew E. Suss [a,*]

[a] Faculty of Mechanical Engineering, Technion – Israel Institute of Technology, Haifa, Israel
[b] Wetsus, European Centre of Excellence for Sustainable Water Technology, Leeuwarden, The Netherlands

HIGHLIGHTS

- A 1D improved modified Donnan model is developed for flow-through electrode cell architecture
- Suitable fitting parameters are obtained via fitting model to equilibrium charge and salt stored data from a custom-built cell.
- Model well-describes dynamic effluent salt concentration and cell current data, showing that flow-through CDI can be described with simpler 1D models.

ARTICLE INFO

Article history:
Received 13 November 2016
Received in revised form 22 January 2017
Accepted 8 March 2017
Available online 10 April 2017

ABSTRACT

Capacitive deionization (CDI) is a fast-emerging water desalination technology in which a small cell voltage of ~1 V across porous carbon electrodes removes salt from feedwaters via electrosorption. In flow-through electrode (FTE) CDI cell architecture, feedwater is pumped through macropores or laser perforated channels in porous electrodes, enabling highly compact cells with parallel flow and electric field, as well as rapid salt removal. We here present a one-dimensional model describing water desalination by FTE CDI based on modified Donnan electric double layer theory, and employing simple cell boundary conditions derived via scaling arguments. We further provide a comparison of model results to data obtained from a custom-built FTE CDI cell. We show good model-to-equilibrium data fits with reasonable values for fitting parameters such as the Stern layer capacitance, micropore volume, and attraction energy. Further, the model well-describes dynamic effluent salt concentration and cell current obtained from the experimental cell. Thus, we demonstrate that from an engineering modeling perspective, an FTE CDI cell can be described with simpler one-dimensional models, unlike more typical flow-between electrodes architecture where 2D models are required.

1. Introduction

Capacitive deionization (CDI) is a rapidly growing research field, with primary applications in brackish water desalination and wastewater purification [1]. A CDI cell typically consists of two carbon-based porous electrodes that are electronically isolated by a separator, and feedwater is pumped through the cell. Applying a voltage across the electrodes causes charged ions in the feed to migrate to oppositely charged electrodes and to be electrostatically contained in electric double layers (EDLs) within micropores [2,3]. This process constitutes the charge half-cycle, and is also the desalination stage. Once the electrodes are fully charged, they can be discharged by short circuiting the electrodes, allowing the stored ions to be released into the flow and resulting in a waste brine stream. A number of CDI cell architectures have been developed [4–7], but the earliest and most common architecture is composed of two electrodes separated by a separator channel, through which the feedwater is pumped. This architecture is often referred to as flow-by or flow-between electrodes (FB) [1].

An alternative CDI cell architecture is the flow-through electrode (FTE) architecture, where the feedwater flows directly through electrode macropores rather than between the electrodes (see Fig. 1a) [8–10]. One main advantage of FTE relative to FB is that the electric field and flow directions are parallel, allowing for facile optimization of ionic and flow resistances [8]. Further, since the separator is no longer the main flow channel in an FTE cell, the separator thickness may be minimized (provided the electronic isolation remains adequate), resulting in improved desalination rates and more compact cells [8, 11]. However, it has been reported that anode corrosion occurs at a faster rate in FTE CDI systems relative to FB systems, though nitrogen sparging to reduce dissolved oxygen content in the feedwater has been shown to increase FTE cell stability to a level comparable to FB cells [12]. Further, surface charge modification has been shown to reduce anode corrosion and improve charge efficiency in FTE systems

* Corresponding author.
E-mail address: mesuss@technion.ac.il (M.E. Suss).

http://dx.doi.org/10.1016/j.desal.2017.03.013
0011-9164/

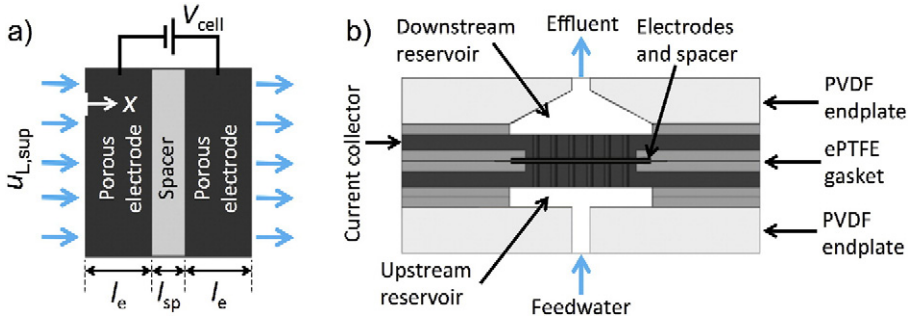

Fig. 1. a) Schematic of the 1D model domain, which includes both electrodes and the spacer. b) Schematic of the experimental FTE CDI cell used in this work, with cell dimensions provided in the Materials and methods section.

[9]. Another potential drawback of FTE is that such cells can require greater feed pressures than FB cells in order to flow through the electrodes' macropores with the desired throughput [8]. However, recent work by Guyes et al. has demonstrated that laser perforating electrodes with roughly 200 μm diameter flow channels enabled orders of magnitude improvement in electrode hydraulic permeability without affecting the electrodes salt adsorption capacity or gravimetric capacitance [13].

Several engineering models for water desalination by CDI have been proposed which couple macroscopic porous electrode theory to an EDL structure model [14–18]. The models developed to date are generally applied to flow-between CDI cells, where flow and electric field are perpendicular, necessitating a 2D model approach [17,18]. Hemmatifar et al. demonstrated the first fully 2D model for flow-between CDI cells, which employed a Donnan EDL model [18]. A widely-applied model utilizes a modified Donnan theory to describe the EDL in micropores of CDI electrodes, and which demonstrates good fits to data over a wide range of experimental conditions and electrode materials [19,20]. While FTE CDI is a promising CDI cell architecture, to our knowledge there has not been a comparison between FTE CDI data to an appropriate model. We here develop a 1D model and simplified boundary conditions for FTE CDI cells, employing a modified Donnan EDL model. We further present the fitting of our model to FTE CDI data from a custom-built cell.

2. Theory

To develop a 1D FTE CDI model, we start with the volume-averaged, 1D, superficial molar flux of an ion, J_i, given by the extended Nernst-Planck equation,

$$J_i = c_{mA,i}\cdot\nu - D_{mA,i}\cdot\left(\frac{\partial c_{mA,i}}{\partial x} + z_i c_{mA,i}\frac{\partial \phi_{mA}}{\partial x}\right) \tag{1}$$

where $c_{mA,i}$ is the ion concentration in the macropores of the electrode (defined as a concentration per unit macropore volume), ν is the superficial fluid velocity of the electrolyte phase, $D_{mA,i}$ is an effective ion diffusion coefficient, z_i is the ion valence, ϕ_{mA} is the dimensionless macropore electric potential (which can be multiplied by the thermal voltage $V_T = RT/F$ to arrive at a dimensional voltage), and x is a spatial coordinate along the flow and electric field direction in our model FTE CDI cell (see Fig. 1a). The effective ion diffusion coefficient in the electrodes, $D_{mA,i} = p_{mA}D_{\infty,i}/\tau_{mA}$, where $D_{\infty,i}$ is the ion's molecular diffusivity, includes a correction for macropore porosity, p_{mA}, and tortuosity, τ_{mA}. For simplicity, we assume a binary electrolyte with univalent ions and equal cation and anion diffusivities, whereas future works will investigate the effect of more complex electrolyte solutions.

A conservation of species applied to anion or cation yields

$$\frac{\partial c_{eff,i}}{\partial t} = -\frac{\partial J_i}{\partial x}\ ,\ c_{eff,i} = p_{mA}c_{mA,i} + p_{mi}c_{mi,i} \tag{2}$$

where p_{mi} is the porosity of the electrode's micropores. We combine Eqs. (1) and (2) to arrive at salt and charge balance equations, given by

$$\begin{aligned} \frac{\partial c_{eff}}{\partial t} &= -\nu\cdot\frac{\partial c_{mA}}{\partial x} + D_{mA}\cdot\frac{\partial^2 c_{mA}}{\partial x^2}\ ,\ c_{eff} = p_{mA}c_{mA} + \frac{1}{2}p_{mi}c_{mi,ions} \\ p_{mi}\frac{\partial \sigma_{ionic}}{\partial t} &= 2\cdot D_{mA}\cdot\frac{\partial}{\partial x}\left(c_{mA}\frac{\partial \phi_{mA}}{\partial x}\right) \end{aligned} \tag{3}$$

where c_{mA} is the macropore salt concentration ($= c_{mA,+} = c_{mA,-}$ by electroneutrality), $c_{mi,ions}$ is the total ion concentration in the micropores ($= c_{mi,+} + c_{mi,-}$), and σ_{ionic} is the ionic micropore charge ($= c_{mi,+} - c_{mi,-}$).

Micropores in porous CDI electrodes are responsible for salt electrosorption and present a highly confined geometry. One method for modeling the EDL structure within such confined geometry is a Donnan or modified Donnan approach [21]. In the Donnan approach, the potential in the micropore volume is assumed to be constant, independent of the distance to the carbon wall. Furthermore, assuming that ion transport between micropores and macropores (those at the same x-position) is rapid and so transport across the electrode thickness is rate limiting, Boltzmann's law relates ion concentrations in micro- and macropore volumes,

$$c_{mi,i} = c_{mA,i}\cdot\ \exp(-z_i\cdot\Delta\phi_D + \mu_{att}) \tag{4}$$

where $\Delta\phi_D$ is the (dimensionless) Donnan potential, defined as the potential within the volume of micropores relative to that in adjacent macropores. An empirical ion attraction term μ_{att} is used which aids in fitting of the theory to data (μ_{att} is assumed to be the same for both ions), which is an inverse function of total micropore ions concentration, $\mu_{att} = E/c_{ions,mi}$, with E a constant micropore attraction energy [22]. This approach has the advantage of relative mathematical simplicity and a good fit of data to theory [20,22]. More recent theories model the EDL structure without the use of a term μ_{att}, instead including charged surface groups in the micropores, termed an amphoteric Donnan model [23].

For the modified Donnan EDL model, mobile ionic charge in the micropores, σ_{ionic}, is equal in magnitude to the electronic charge, σ_{elec}, which resides in the carbon matrix surrounding the micropore, $\sigma_{ionic} + \sigma_{elec} = 0$. When anode and cathode have the same size and microporosity, the thickness-averaged electronic charge in one electrode is equal in magnitude to the average electronic charge in the other electrode: $\langle\sigma_{elec,A}\rangle + \langle\sigma_{elec,C}\rangle = 0$. In this case, we can relate the ionic current density in the separator layer, J_{ch}, to the averaged electrode

charge as

$$p_{mi}\frac{\partial\langle\sigma_{elec,j}\rangle}{\partial t}=\pm\frac{J_{ch}}{L_{elec}} \tag{5}$$

where the sign, ±, depends on the electrode. The EDL model is completed with the following equations, solved together with the PDEs (Eq. (3)) at each x-position,

$$c_{ions,mi}^2=\sigma_{ionic}^2+(2c_{mA}e^{\mu_{att}})^2$$
$$\phi_1-\phi_{mA}=\Delta\phi_D+\Delta\phi_S=-\sinh^{-1}(\sigma_{ionic}/(2c_{mA}e^{\mu_{att}}))-\sigma_{ionic}\cdot F/(C_SV_T) \tag{6}$$

where C_S is the volumetric Stern layer capacitance, and ϕ_1 is the solid phase (carbon) potential. The cell voltage is $V_{cell}=V_T\cdot(\phi_{1,A}-\phi_{1,C})$, where A and C refer to anode and cathode.

For the spacer, we use Eq. (3) with $p_{mi}=0$ and p_{mA} replaced by p_{sp}. Note that the effective diffusion coefficient is different in the electrode and spacer due to pore structure differences, see Table 1. At the electrode-spacer interfaces, $x=l_e$ and $x=l_e+l_{sp}$, where l_e is the electrode thickness and l_{sp} is the spacer thickness (see Fig. 1a), the continuity of salt flux results in

$$D_{mA}\frac{\partial c_{mA}}{\partial x}\bigg|_{x=l_e,l_e+l_{sp}}=D_{sp}\frac{\partial c_{sp}}{\partial x}\bigg|_{x=l_e,l_e+l_{sp}}. \tag{7}$$

Because of continuity of the current, the current density across the spacer, J_{ch}, is given by

$$J_{ch}=-2D_{sp}c_{sp}\frac{\partial\phi_{sp}}{\partial x}. \tag{8}$$

Eq. (8) can be integrated to yield

$$J_{ch}\cdot\int_{l_e}^{l_e+l_{sp}}c_{sp}^{-1}\,dx=-2D_{sp}\cdot\left[\phi_{sp}(x=l_e+l_{sp})-\phi_{sp}(x=l_e)\right]. \tag{9}$$

To derive boundary conditions for the upstream end of our FTE CDI cell ($x=0$), we begin with a balance of salt applied to a long upstream reservoir,

$$\frac{\partial}{\partial t}\left[\int_{res}c_{res}\,dx\right]=\nu\,[c_{feed}-c_{mA}(x=0)]+D_{mA}\frac{\partial c_{mA}}{\partial x}\bigg|_{x=0}. \tag{10}$$

Since the reservoir is long, the concentration at the upstream end of the reservoir is unperturbed by the desalination process and remains fixed at the feed concentration, c_{feed}. In Eq. (10), the integral in the left-hand side is over the length of the upstream reservoir, and c_{res} is the local concentration in the upstream reservoir. Eq. (10) takes into account the advection of salt into and out of the reservoir, the diffusion of salt into the upstream electrode of the FTE CDI cell, and local changes in concentration in the reservoir as a result of salt diffusion. A concentration boundary layer forms in the reservoir at the upstream reservoir/electrode interface due to the diffusion of salt into the salt-depleted electrode pore space. Taking the limit of high Peclet number, $Pe=\nu l_e/D_{mA}\gg1$, the concentration boundary layer thickness, δ, becomes much smaller than the geometric length scale so that $\varepsilon\equiv\delta/l_e\ll1$. If we now restrict the reservoir domain to only the boundary layer, we can scale Eq. (10) using $c^*\equiv c/c_{feed}$, $t^*=tD_{mA}/l_e^2$, and $x^*\equiv x/\delta$, to obtain

$$Pe^{-1}\,\frac{\partial}{\partial t^*}\left[\int_{res}c_{res}^*\,dx^*\right]=\frac{1}{\varepsilon}\,\left[1-c_{mA}^*(x=0)\right]+\frac{1}{\varepsilon^2Pe}\,\frac{\partial c_{mA}^*}{\partial x^*}\bigg|_{x=0}. \tag{11}$$

The time scaling used in Eq. (11) is the characteristic timescale for desalination by a CDI cell [24], as this desalination is what drives salt removal from the upstream reservoir. For $Pe\gg1$ and so $\varepsilon\ll1$ (for our experimental cell, Pe ~ 25), we can neglect the left-hand side term in Eq. (11). Thus, we obtain a simple boundary condition for concentration which we employ at the upstream end of the model cell, $x=0$,

$$0=\nu\,[c_{feed}-c_{mA}(x=0)]+D_{mA}\frac{\partial c_{mA}}{\partial x}\bigg|_{x=0}. \tag{12}$$

On the downstream end of the cell ($x=2l_e+l_{sp}$), salt transport between the electrode and downstream reservoir is due to advection and diffusion. Unlike at the upstream end, a thin concentration boundary layer is not expected to form in the downstream reservoir. As a result, for conditions of high Pe, diffusive flux of salt at the interface is much smaller than advective flux. Thus, we here neglect the diffusive flux, and apply a boundary condition at the downstream end of the cell of $\partial c_{mA}/\partial x|_{x=2l_e+l_{sp}}=0$. The boundary conditions applied at the upstream and downstream ends of the cell for potential are $\partial\phi_{mA}/\partial x|_{x=0,2l_e+l_{sp}}=0$, as no ionic current leaves or enters the cell and we assumed equal ion diffusivities.

Finally, we also include in our model a mixing tank and a plug flow reactor downstream of the cell in order to capture the presence in experimental systems of liquid volume downstream of the CDI cell until the conductivity sensor (~1 mL for our experimental system, see Materials and methods section). In this volume, mixing and dispersion can act to reduce concentration gradients, affecting cell effluent concentration measurements. The model for the mixing tank after the cell is given by

$$t_{mix}\frac{\partial c_{cs}}{\partial t}=c(x=2l_e+l_{sp})-c_{cs} \tag{13}$$

where t_{mix} is the average residence time in the mixing tank (given by its volume divided by volumetric flow rate), and c_{cs} is the concentration as sensed by the conductivity sensor. The plug flow reactor simply institutes a time-delay, t_{plug}, of the effluent conductivity profile.

Table 1
List of model parameters and their values.

Model parameter	Value
ρ_{elec}: electrode mass density	0.25 g/mL
v_{mi}: specific volume of micropores	0.55 mL/g (fitting parameter)
p_{mi}: microporosity	$\rho_{elec}\cdot v_{mi}=0.1375$
p_{sk}: "carbon skeleton"	$\rho_{elec}/p_{sk}=01316$ (p_{sk} ~ 19 g/mL)
p_{mA}: mAcroporosity	$1-p_{mi}-p_{sk}=0.7309$
E: ion attraction energy	700 mol/m^3 (fitting parameter)
C_S: Stern capacity	145 F/m^2 (fitting parameter)
l_e: electrode thickness	500 μm
l_{sp}, p_{sp}: spacer thickness and porosity	260 μm, 0.85
ν: superficial velocity	66.4 μm/s
t_{pc-mv}: mixing vessel retention time	60 s
t_{plug}: plug flow reactor time	15 s
D_∞: ion diffusivity	$D_\infty=(D_{Na}+D_{Cl})/2=1.68\cdot10^{-9}$ m^2/s
D: effective diffusion coefficients	$D_{mA}=D_\infty\cdot p_{mA}/\tau_{mA}$, $D_{sp}=D_\infty\cdot p_{sp}/\tau_{sp}$
τ: tortuosity	$\tau_{mA/sp}=1/p_{mA/sp}^{1/2}$ (Bruggeman equation)

3. Materials and methods

The FTE CDI cell (Fig. 1b) consists of a pair of commercial porous activated carbon woven-fiber electrodes (ACC-507-15, Kynol Europa GmbH, ~500 μm thickness each, 1.75 × 1.75 cm^2). A porous separator (GE Life Sciences, Whatman GF/A borosilicate glass filter paper, 260 μm thickness, 2.4 × 2.4 cm^2) electronically isolates the electrodes. ePTFE gaskets (W.L. Gore & Associates, Gore-Tex NSG16X-GP, 1.4 mm uncompressed thickness, 5 × 5 cm^2) are used to seal the cell, while a laser-cut square in the gasket (1.55 × 1.55 cm^2) permits feedwater to

pass through the electrodes and separator. The electrodes fit tightly into grooves laser-cut on the aperture perimeter, preventing feedwater from leaking around the electrode edges. The upstream negative current collector is milled from a resin-filled impervious graphite (FC-GR, Graphitestore.com, Inc., Buffalo Grove, IL, USA), which prevents water leakage through the graphite's structure. The downstream positive collector is milled from isomolded graphite (GM-10, Graphitestore.com), where leak protection is unnecessary due to lower hydraulic pressures. The current collectors both contain an array of cylindrical channels (6 × 6 grid, 1.5 mm diameter, 3 mm length) that allow water to pass through, and tabs to enable electrical contact with the voltage source. Water reservoirs are created upstream and downstream of the collectors via two ePTFE gaskets on the upstream side and a single ePTFE gasket and pyramidal contraction on the downstream side (the latter is ground by hand with a Dremel cutting tool into the downstream endplate). The downstream reservoir components have a combined volume of ~0.5 mL. The cell terminates on either side with endplates milled from PVDF (5 × 5 cm^2) that each include one fluid flow line and one vent that allows air removal from the cell. Effluent enters the outlet line with a tube volume totaling 0.5 mL between the endplate and downstream conductivity sensor. The cell is sealed with 8 bolts (M4 × 30 mm) tightened to 35 N·cm which are electrically isolated from the graphite current collectors via shrink tubing.

For desalination experiments, feedwater (NaCl 5 mM or 20 mM concentration) was drawn at 1 mL/min from a glass bulk reservoir by the peristaltic pump and fed into the CDI cell via semi-rigid polyethylene tubing. A fresh electrode pair was used for each feedwater concentration, and the total dry mass of each pair was 0.078 g and 0.077 g for 5 mM and 20 mM concentrations, respectively. The cell effluent was then fed into a conductivity cell (5-ring, Metrohm, Inc., Switzerland) with a custom-milled insert to reduce the internal volume, and then returned to the bulk reservoir. The bulk reservoir volume (~2 L) was significantly larger than the volume of the rest of the setup (~20 mL) in order to maintain constant concentration in the reservoir throughout experiments. During the charging half-cycle of the desalination experiments, a constant voltage of between 0.2 and 1.2 V was applied to the cell by a voltage source (SourceMeter 2400, Keithley Instruments, Inc., Solon, OH, USA), while during the discharging half-cycle a cell voltage of 0 V was maintained.

4. Results and discussion

The first step towards comparison of data to the model is to fit equilibrium data of charge stored and salt adsorption capacity (eq-SAC) to the equilibrium results of the model. Data was taken with our custom-built FTE CDI cell operated in constant voltage mode, where the charge half-cycle was continued until equilibrium. Equilibrium occurred when the effluent concentration returned to the feed concentration and the current decreased to reach a steady value (leakage current). Charge stored was obtained by integrating the cell's current response during the discharge half-cycle. Eq-SAC was obtained by integrating the difference between feed and effluent concentration during the charge half-cycle, multiplied by the feed flow rate. It is useful to express charge stored and eq-SAC as mass-specific quantities, meaning that they are divided by the total mass of the electrode pair used in the experiment, allowing for a ready comparison between various electrode materials.

The results of the fitting are shown in Fig. 2a and b, and as can be seen, model-to-data fitting gave good agreement for fitting parameters of $\nu_{mi} = 0.55$ g/mL, $E = 700$ kT·mol/m^3 and $C_S = 145$ F/mL. These values are similar to those obtained from equilibrium model-to-data fitting for other CDI electrode materials, though the value for E is at least twice higher than previously reported [22,25]. The latter may be due to slight variations in the micropore size of the electrode material used here compared to those used previously, since the parameter E is expected to scale as λ_p^{-4}, where λ_p is micropore size [22]. Fig. 2c also shows a model-to-data comparison for the equilibrium value of the

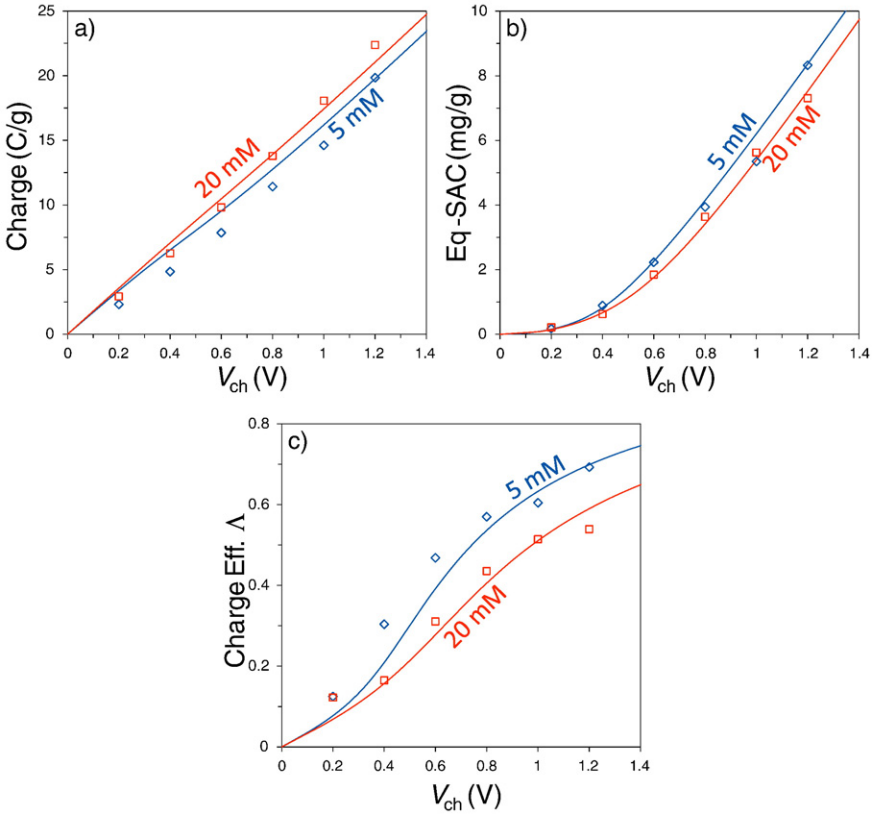

Fig. 2. Results of model-to-data fitting for several measured cell parameters at equilibrium including a) charge stored per gram of electrode material, b) equilibrium salt adsorption capacity per gram of electrode material (eq-SAC), and c) charge efficiency, as functions of charging voltage V_{ch}.

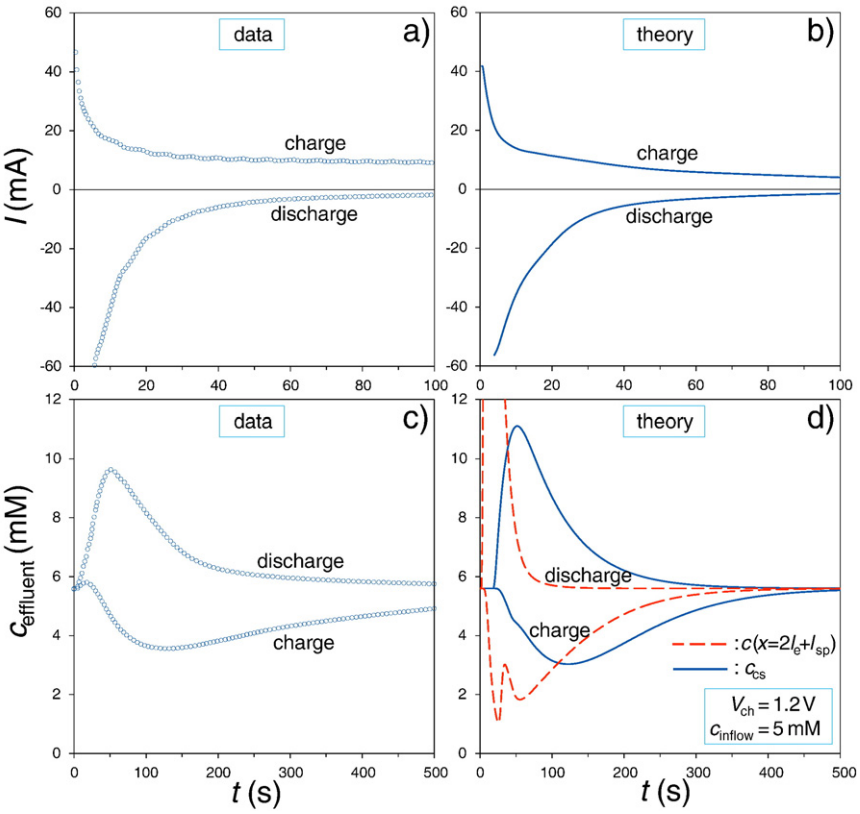

Fig. 3. Comparison of model results to data for the charge half-cycle, c_{inflow} = 5 mM NaCl, and V_{ch} = 1.2 V. a) and b) represent the comparison for current response of the CDI cell, while c) and d) are for the cell effluent concentration of the CDI cell, and c_{cs} refers to the conductivity predicted at the location of a downstream conductivity sensor.

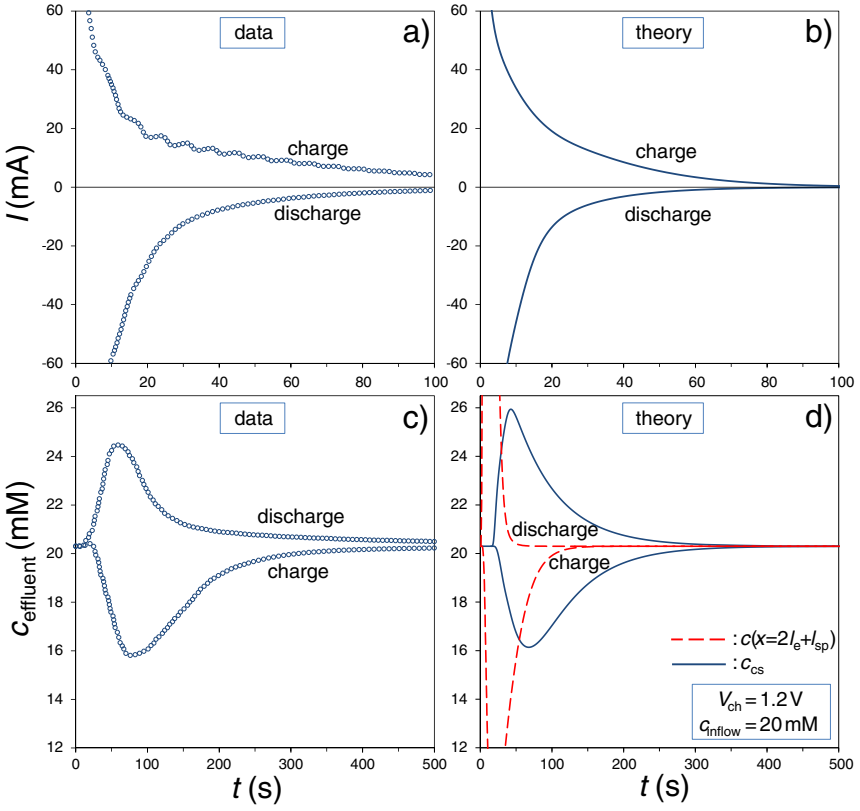

Fig. 4. Comparison of model results to data for the charge half-cycle, c_{inflow} = 20 mM NaCl, and V_{ch} = 1.2 V. a) and b) represent the comparison for current response of the CDI cell, while c) and d) are for the cell effluent concentration of the CDI cell, and c_{cs} refers to the conductivity predicted at the location of a downstream conductivity sensor.

parameter charge efficiency, which is defined as the moles of salt stored in the electrodes to the moles of electrons stored [1]. Charge efficiency of our experimental cell varied from ~0.1 at a cell voltage of 0.2 V to roughly 0.7 at 1.2 V for the case of 5 mM feed concentration, similar to the trends predicted by the model.

After determining the fitting parameters from equilibrium model-to-data fitting, we could compare dynamic model and data results, which is done in Fig. 3 for the case of 5 mM NaCl feedstream and Fig. 4 for the case of 20 mM NaCl feedstream. In Figs. 3 and 4, we can see good qualitative and quantitative agreement between model results and data when including the effect of the downstream volume in our cell (Eq. (13)). Good agreements are obtained for both the cell's current response (I, Figs. 3a and b and 4a and b) and effluent concentration ($c_{effluent}$, Figs. 3c and d and 4c and d), and for both the charge and the discharge half-cycles. Thus, we conclude that 1D models can be used to describe experimental data from FTE CDI cells, unlike FB CDI cells which necessarily require 2D models. Also shown in Figs. 3d and 4d is the predicted effluent concentration when excluding the effect of the downstream volume in the model (red dashed lines), which shows sharper features and poor comparison to the experimental data (Figs. 3c and 4c). The latter demonstrates the importance of accounting for the electrolyte volume and diffusion effects downstream of the cell in predicting the effluent concentration at the location of the conductivity sensor in FTE CDI cells. An interesting feature seen in the red dashed line of Fig. 3d representing the charge half-cycle is an initial sharp decrease in effluent concentration, followed by a sharp rise, then another sharp decay, and finally followed by slow rise to the feedwater concentration. Such complex behavior is unique to FTE CDI cells, and occurs at early times in the charging process, when the electrodes' pore space is significantly desalted via electrosorption while the separator pore space is less desalted. Advection at conditions of high Peclet number through the cell at these early times causes the oscillatory effluent concentration as water from the electrodes (desalted) and separator (less desalted) is advected out. The downstream volume of our experimental cell induces additional diffusion within the effluent, which is predicted to obfuscate these unique dynamics (see blue curve in Fig. 3d). However, future optimization of FTE CDI cells for minimized downstream volume may allow for direct measurements of such features in the effluent concentration, which could allow for significant insights into the relative desalination performance of the downstream electrode versus the upstream electrode.

5. Conclusions

In conclusion, we present a model for flow-through electrode capacitive deionization (FTE CDI) based on modified Donnan EDL structure model and porous electrode transport theory. Although possessing similarities to models for flow-between CDI cells, our model was unique in that a simple one-dimensional approach was able to capture experimental results, and simple boundary conditions derived via scaling arguments were developed. Model-to-data comparisons showed good qualitative agreement when including the effect of a significant volume downstream of the cell. Future work can model other features important to desalination by FTE CDI, such as pH variations in the cell effluent and the effects of charged surface groups in porous electrodes.

Acknowledgements

We would like to acknowledge funding from the Israeli Ministry of National Infrastructures, Energy and Water Resources.

References

[1] M.E. Suss, et al., Water desalination via capacitive deionization: what is it and what can we expect from it? Energy Environ. Sci. 8 (2015) 2296–2319.
[2] M. Mirzadeh, F. Gibou, T.M. Squires, Enhanced charging kinetics of porous electrodes: surface conduction as a short-circuit mechanism, Phys. Rev. Lett. 113 (2014) 97701.
[3] R.A. Rica, R. Ziano, D. Salerno, F. Mantegazza, D. Brogioli, Thermodynamic relation between voltage-concentration dependence and salt adsorption in electrochemical cells, Phys. Rev. Lett. 109 (2012) 156103.
[4] S. Jeon, et al., Desalination via a new membrane capacitive deionization process utilizing flow-electrodes, Energy Environ. Sci. 6 (2013) 1471–1475.
[5] J. Lee, S. Kim, C. Kim, J. Yoon, Hybrid capacitive deionization to enhance the desalination performance of capacitive techniques, Energy Environ. Sci. 7 (2014) 3683–3689.
[6] X. Gao, A. Omosebi, J. Landon, K. Liu, Surface charge enhanced carbon electrodes for stable and efficient capacitive deionization using inverted adsorption–desorption behavior, Energy Environ. Sci. 8 (2015) 897–909.
[7] P. Srimuk, et al., MXene as a novel intercalation-type pseudocapacitive cathode and anode for capacitive deionization, J. Mater. Chem. A 4 (2016) 18265–18271.
[8] M.E. Suss, et al., Capacitive desalination with flow-through electrodes, Energy Environ. Sci. 5 (2012) 9511–9519.
[9] I. Cohen, E. Avraham, M. Noked, A. Soffer, D. Aurbach, Enhanced charge efficiency in capacitive deionization achieved by surface-treated electrodes and by means of a third electrode, J. Phys. Chem. C 115 (2011) 19856–19863.
[10] A.M. Johnson, J. Newman, Desalting by means of porous carbon electrodes, J. Electrochem. Soc. 118 (1971) 510–517.
[11] Y. Qu, et al., Energy consumption analysis of constant voltage and constant current operations in capacitive deionization, Desalination 400 (2016) 18–24.
[12] I. Cohen, E. Avraham, Y. Bouhadana, A. Soffer, D. Aurbach, The effect of the flow-regime, reversal of polarization, and oxygen on the long term stability in capacitive de-ionization processes, Electrochim. Acta 153 (2015) 106–114.
[13] E.N. Guyes, A. Simanovski, M.E. Suss, Several Orders of Magnitude Increase in Hydraulic Permeability of Flow-through Capacitive Deionization Electrodes Via Laser Perforations, 2017 In press, RSC Advances.
[14] P.M. Biesheuvel, H.V.M. Hamelers, M.E. Suss, Theory of water desalination by porous electrodes with immobile chemical charge, Colloid Interface Sci. Commun. 9 (2015) 1–5.
[15] J. Gabitto, C. Tsouris, Volume averaging study of the capacitive deionization process in homogeneous porous media, Transp. Porous Media 109 (2015) 61–80.
[16] A. Shocron, M.E. Suss, The effect of surface transport on water desalination by porous electrodes undergoing capacitive charging, J. Phys. Condens. Matter 29 (2017) 84003.
[17] W. Tang, P. Kovalsky, B. Cao, T.D. Waite, Investigation of fluoride removal from low-salinity groundwater by single-pass constant-voltage capacitive deionization, Water Res. 99 (2016) 112–121.
[18] A. Hemmatifar, M. Stadermann, J.G. Santiago, Two-dimensional porous electrode model for capacitive deionization, J. Phys. Chem. C 119 (2015) 24681–24694.
[19] X. Gao, et al., Complementary surface charge for enhanced capacitive deionization, Water Res. 92 (2016) 275–282.
[20] T. Kim, et al., Enhanced charge efficiency and reduced energy use in capacitive deionization by increasing the discharge voltage, J. Colloid Interface Sci. 446 (2015) 317–326.
[21] P.M. Biesheuvel, Y. Fu, M.Z. Bazant, Electrochemistry and capacitive charging of porous electrodes in asymmetric multicomponent electrolytes, Russ. J. Electrochem. 48 (2012) 580–592.
[22] P.M. Biesheuvel, S. Porada, M. Levi, M.Z. Bazant, Attractive forces in microporous carbon electrodes for capacitive deionization, J. Solid State Electrochem. 18 (2014) 1365–1376.
[23] P.M. Biesheuvel, Activated Carbon Is an Electron-conducting Amphoteric Ion Adsorbent, 2015 (arXiv Prepr. arXiv1509.06354).
[24] P.M. Biesheuvel, M.Z. Bazant, Nonlinear dynamics of capacitive charging and desalination by porous electrodes, Phys. Rev. E 81 (2010) 31502.
[25] J.E. Dykstra, R. Zhao, P.M. Biesheuvel, A. Van der Wal, Resistance identification and rational process design in Capacitive Deionization, Water Res. 88 (2016) 358–370.